OXFORD

ARTICLE

Tegavivint and the β-Catenin/ALDH Axis in Chemotherapy-Resistant and Metastatic Osteosarcoma

Motonari Nomura, Nino Rainusso, Yi-Chien Lee, Brian Dawson, Cristian Coarfa, Ruolan Han, Jeffrey L. Larson, Ryan Shuck, Lyazat Kurenbekova, Jason T. Yustein

See the Notes section for the full list of authors' affiliations.
Correspondence to: Jason T. Yustein, MD, PhD, Department of Pediatrics, Texas Children's Cancer and Hematology Center, Baylor College of Medicine, Houston, TX (e-mail: yustein@bcm.edu).

Abstract

Background: The Wnt/β-catenin pathway is closely associated with osteosarcoma (OS) development and metastatic progression. We investigated the antitumor activity of Tegavivint, a novel β-catenin/transducin β-like protein 1 (TBL1) inhibitor, against OS employing in vitro, ex vivo, and in vivo cell line and patient-derived xenograft (PDX) models that recapitulate high risk disease.

Methods: The antitumor efficacy of Tegavivint was evaluated in vitro using established OS and PDX-derived cell lines. Use of an ex vivo three-dimensional pulmonary metastasis assay assessed targeting of β-catenin activity during micro- and macro-metastatic development. The in vivo activity of Tegavivint was evaluated using chemoresistant and metastatic OS PDX models. Gene and protein expression were quantified by quantitative Reverse transcription polymerase chain reaction or immunoblot analysis. Bone integrity was determined via microCT. All statistical tests were two-sided.

Results: Tegavivint exhibited antiproliferative activity against OS cells in vitro and actively reduced micro- and macrometastatic development ex vivo. Multiple OS PDX tumors (n = 3), including paired patient primary and lung metastatic tumors with inherent chemoresistance, were suppressed by Tegavivint in vivo. We identified that metastatic lung OS cell lines (n = 2) exhibited increased stem cell signatures, including enhanced concomitant aldehyde dehydrogenase (ALDH1) and β-catenin expression and downstream activity, which were suppressed by Tegavivint (ALDH1: control group, mean relative mRNA expression = 1.00, 95% confidence interval [CI] = 0.68 to 1.22 vs Tegavivint group, mean = 0.011, 95% CI = 0.0012 to 0.056, P < .001; β-catenin: control group, mean relative mRNA expression = 1.00, 95% CI = 0.71 to 1.36 vs Tegavivint group, mean = 0.45, 95% CI = 0.36 to 0.52, P < .001). ALDH1^{high} PDX-derived lung OS cells, which demonstrated enhanced metastatic potential compared with ALDH^{low} cells in vivo, were sensitive to Tegavivint. Toxicity studies revealed decreased bone density in male Tegavivint-treated mice (n = 4 mice per group).

Conclusions: Tegavivint is a promising therapeutic agent for advanced stages of OS via its targeting of the β-catenin/ALDH1 axis.

Osteosarcoma (OS) is the most common malignant bone tumor in the pediatric population. Approximately 25% of patients present with detectable metastases, most frequently in the lungs (1). Although incorporation of multidrug chemotherapy has improved the prognosis, patients with metastatic or refractory disease have extremely poor prognosis. And although there have not been reported mutations in β-catenin in OS, the activation

of β-catenin is closely associated with the progression and chemoresistance of OS (2–13) via effects on downstream target genes, such as c-Myc, implying that β-catenin-mediated signaling can be a therapeutic target for metastatic OS.

Tegavivint, also known as BC2059, was discovered during a phenotypic screen for inhibitors of Wnt/β-catenin signaling (15). It is currently in clinical development with the first-in-human

clinical trial being conducted in patients with desmoid tumors, which have increased β-catenin activity (14). Tegavivint directly and selectively interferes with the interaction between β-catenin and transducin β-like protein 1 (TBL1) and TBL receptor 1 (TBLR1). Disruption of β-catenin-TBL1/TBLR1 binding inhibits β-catenin nuclear translocation and promotes its degradation. Recently, Tegavivint has shown antitumor activity preclinically against acute myeloid leukemia (16) and multiple myeloma (17) in vitro and in vivo; however, there is no published evidence to support its antitumor efficacy against malignant solid tumors.

The Wnt/β-catenin pathway also regulates tissue self-renewal, a feature of tumor stem cells, which have been identified in sarcomas using different markers, including enhanced aldehyde dehydrogenase (ALDH1) activity (18,19), and the ability to resist chemotherapy and initiate metastasis (20). Therefore, we hypothesized that pharmacological targeting of β-catenin could have statistically significant antitumor activity for chemoresistant and metastatic OS. Our goals were to examine the effects of pharmacological inhibition of β-catenin activity on self-renewal and metastatic-initiating capabilities.

Using a panel of OS cell lines and patient-derived xenograft (PDX) models that represent high-risk disease, including therapeutic-resistant and metastatic disease, we investigated the efficacy of Tegavivint in targeting OS in vitro, ex vivo, and in vivo.

Methods

In Vivo Tumor Xenotransplantation and Metastasis

For orthotopic models, 1×10^6 viable LM7 cells transduced with the 7TGC vector (LM7-7TGC) were injected into the left tibia bone of 6-week-old male or female NOD-SCID-IL2$\gamma^{-/-}$ (NSG) mice. Treatment with intraperitoneal (i.p.) injection of 50 mg/kg Tegavivint or 5% dextrose for three males and two females per group was initiated when the tumor volume reached approximately 100 mm^3. Tumor volume was measured in a blinded manner with electric calipers as tumor volume (mm^3) = long diameter $\times$ (short diameter)^2/2.

For subcutaneous models, TCCC-OS22 or TCCC-OS63 tumor slices (approximately 3 mm per side) were implanted in the hind flank of 6-week-old NSG mice (TCCC-OS22: three males and two females per group, TCCC-OS63: two males and two females per group). When the tumor volume reached approximately 100 mm^3, i.p. injection of 5% dextrose, Tegavivint, doxorubicin, or the combination of doxorubicin and Tegavivint was initiated. Mice were euthanized on day 29 or when tumor diameter reached 1.5 cm.

For metastatic tumor models, untreated TCCC-OS84 cells or LM7 cells ALDH1^{high} cells or ALDH1^{low} cells were sorted by flow cytometry. For PDX TCCC-OS84, tumors were dissociated into single cells using the GentleMACS kit (Miltenyi Biotec, Auburn, CA). Cells were injected via tail vein into 6-week-old male or female NSG mice. After 1 week, 5% dextrose or Tegavivint was i.p. injected twice weekly for 4 weeks (three males and two females per group). After an additional 4 weeks without treatment, mice were euthanized and evaluated for metastatic disease.

At necropsy, tumors and lungs were fixed and paraffin-embedded tissues were visualized with hematoxylin and eosin (H&E) staining. All mouse experiments were conducted according to IACUC protocols after approval from the BCM Institutional Review Board (BCM Animal Protocol AN-5225).

Ex vivo Pulmonary Metastasis Assay (PuMA)

Medium1 was prepared by mixing 2$\times$ M-199 (Invitrogen, Carlsbad, CA), 2 μg/mL crystalline bovine insulin (Sigma-Aldrich, St. Louis, MO), 0.2 μg/mL hydrocortisone (Sigma-Aldrich), 0.2 μg/mL retinyl acetate (Sigma-Aldrich), 200 U/mL penicillin, 200 μg/mL streptomycin, and 15% sodium bicarbonate (Invitrogen). Medium2 was prepared by mixing M-199, 1 μg/mL crystalline bovine insulin, 0.1 μg/mL hydrocortisone, 0.1 μg/mL retinyl acetate, 100 U/mL penicillin, 100 μg/mL streptomycin, and 7.5% sodium bicarbonate.

The 7TGC-labeled tumor cells were pretreated with 100 ng/mL recombinant Wnt3a ligand for 3 days. Then, 1×10^6 viable 7TGC-labeled tumor cells with 100 ng/mL Wnt3a ligand were injected into NSG mice via tail vein. Within 15 minutes after injection, mice were euthanized. The chest cavity was exposed, and the trachea was cannulated with a 20 G catheter. Under constant pressure of 20 cm H$_2$O, 1.2 mL of medium1 mixed with 1.2% low-melting agarose solution with 100 ng/mL of Wnt3a ligand was infused into the lung. When the infusion was complete, the lung was extirpated and immediately placed in cold phosphate buffered saline at 4°C for 20 minutes. Next, transverse sections (1–2 mm) from each lung lobe were made using scalpels or scissors, and four lung sections were then placed on a single 1.5-cm $\times$ 0.7-cm sterile Gelfoam (Pfizer-Pharmacia & Upjohn Company, New York, NY) that had been incubated for 2 hours in a tissue culture dish with medium2 (day 0). Lung sections were incubated at 37°C in a humidified atmosphere of 95% air and 5% CO$_2$. Fresh culture medium2 was replaced, and lung tissue sections were turned over with sterile forceps every other day. Wnt3a ligand (100 ng/mL) was added to the culture medium on days 0 and 4, and Tegavivint (100 nM) was added to the culture medium starting on day 7 and subsequently on days 10, 14, and 17. Whole lung images were captured on days 0, 7, 14, 21, and 28 to evaluate the antitumor effect of Tegavivint using a Leica Stereo Microscope (Leica Microsystems, Buffalo Grove, IL).

MicroCT and Bone Histomorphometry

Lumbar vertebrae and femurs were scanned using a Scanco μCT-40 microCT for quantification of trabecular and cortical bone parameters. We analyzed vertebral and femoral trabecular bone parameters using the Scanco analysis software by manually contouring the trabecular bone of vertebral body L4 as well as the distal metaphyseal section of the femur. To compare the bone density measurements, the bone volume-to-total volume ratio was calculated from these scanned images (21,22).

Statistical Analyses

The data are expressed as mean (SD) only for proliferation assays, and the rest of the data are expressed as median with 95% confidence intervals. Differences in relative cell viability and gene expression between groups were tested for statistical significance with a one-way or two-way ANOVA followed by a two-sided Student t test if the sample size per group was five or more and by a Wilcoxon rank sum test if the sample size was four or less. Survival was analyzed using Kaplan-Meier plotting followed by log-rank test. All statistical tests were two-sided and a P value of less than .05 was considered statistically significant except when multiple hypothesis testing correction was performed using the Benjamini-Hochberg (false discovery rate) method as implemented in the R statistical system; false

discovery rate-adjusted probability values of q less than 0.15 were considered statistically significant.

Additional methods are described in the Supplementary Materials (available online).

Results

Effect of β-Catenin Inhibition by Tegavivint on OS Cells in Vitro

The efficacy of Tegavivint in OS was evaluated in vitro using a panel of OS cell lines, PDX-derived cell lines, and normal human fetal osteoblasts (hFOB1.19). Cell cultures were treated with increasing concentrations of Tegavivint for up to 72 hours. All the cell lines, except hFOB1.19, were extremely sensitive to Tegavivint, with a median half-maximal inhibitory concentration value of 19.2 nM at 72 hours (Figure 1, A–C). In established paired cell lines SaOS-2 and LM7, and PDX-derived TCCC-OS63 and TCCC-OS84 (Supplementary Figure 1A, available online), Tegavivint decreased total protein levels of β-catenin and c-Myc (Figure 1D), and nuclear levels of β-catenin (Figure 1E). Interestingly, the PDX-derived cell lines demonstrated minimal sensitivity to chemotherapy (Supplementary Figure 1B, available online) .

Use of an Orthotopic OS Model to Study the Effect of Tegavivint on Primary Tumor Growth and Distal Metastatic Development

To assess the in vivo efficacy of Tegavivint, we injected LM7 cells orthotopically into the left tibia of 5- to 7-week-old NSG mice. Mice were randomized into two groups of five and treated once daily by i.p. injection of Tegavivint or vehicle (5% dextrose; Figure 2A). After 3 weeks of treatment, the Tegavivint group showed an increase in body weight and abdominal fluid, which reflected an accumulation of the nanoparticle formulation. The dose was reduced to 25 mg/kg/d in the fourth week of treatment, and subsequently body weights returned to normal without signs of intolerance.

Tegavivint treatment resulted in curative antitumor efficacy in this model. Although all tumors in the vehicle group continued to increase in size, no palpable tumors remained in the Tegavivint-treated mice after 4 weeks of drug treatment (Figure 2B). Following euthanasia, lung metastasis was evaluated. Five of five animals in the control group and none of the five animals in the treatment group exhibited visible lung metastasis (Figure 2C). Lung tissue sections were examined for metastasis following H&E staining (Figure 2D). The reduction of lung lesions in the treated mice confirmed the antimetastatic activity of Tegavivint (Figure 2E). Tegavivint has strong antitumor efficacy against both primary tumors and lung metastasis in this human metastatic OS model.

Effect of Tegavivint on PDX Chemoresistant and Metastatic Tumors

We next examined the effects of Tegavivint on PDX tumor specimens from patients with a poor response to chemotherapy (Supplementary Table 1, available online). Both TCCC-OS22 and TCCC-OS63 PDX-derived cell lines were moderately or highly resistant to doxorubicin (Supplementary Figure 1B, available online), thus recapitulating the clinical patient response to chemotherapy. TCCC-0S22 tumor fragments were implanted subcutaneously and treated twice weekly via i.p. injection with Tegavivint or vehicle (Figure 3A). Tegavivint treatment effectively inhibited tumor growth, whereas tumors in the control group grew rapidly (Figure 3, B and C). H&E staining of the remaining tumor mass in treated mice showed signs of necrosis and calcification (Figure 3D).

Whereas TCCC-OS22 was extremely sensitive to Tegavivint in vivo, TCCC-OS63 was somewhat less sensitive to Tegavivint in vitro (Figure 1C); however, pretreatment with doxorubicin enhanced the antitumor efficacy of Tegavivint against TCCC-OS63 in vitro (Figure 4A). We subcutaneously implanted sufficient TCCC-OS63 tumor fragments to four groups of mice (four mice per group, two per sex). Group 1 received vehicle, group 2 received Tegavivint twice per week, group 3 received 2 mg/kg doxorubicin once per week, and group 4 received combination therapy consisting of Tegavivint and doxorubicin at the same doses and intervals. All groups were treated via i.p. injection for a total of 4 weeks (Figure 4B). Administration of Tegavivint alone inhibited tumor growth in all treated mice (average [SD] Tegavivint tumor volume = 677 [157] mm^3 vs average [SD] control tumor volume = 1629 [41] mm^3 at day 15), and this efficacy was greater than that observed with doxorubicin alone (average [SD] doxorubicin tumor volume = 918 [91] mm^3 with survival of only three of four mice in this group by day 15). Among mice in the combination group, three of four tumors remained with stable disease, and only one measurably progressed in size (average [SD] tumor volume = 249 [244] mm^3; Figure 4C). Although Tegavivint alone exerts antitumor activity, this drug can enhance activity in combination with doxorubicin.

Event-free survival analysis revealed differences among the four groups, reflecting the mean tumor volumes. Tegavivint alone resulted in survival of three of four mice on day 26 and one of four mice at study termination (Figure 4D). The combination of Tegavivint with doxorubicin resulted in survival of all mice to study termination. H&E staining showed tumors with enhanced calcification in Tegavivint-treated groups (Figure 4E), and analysis of mRNA expression in the tumor tissue demonstrated statistically significant downregulation of β-catenin (control group, mean relative mRNA expression = 1.00, 95% CI = 0.71 to 1.36 vs Tegavivint group mean = 0.45, 95% CI = 0.36 to 0.52, P < .001) and the Wnt signaling pathway target genes ALDH1 (control group, mean relative mRNA expression = 1.00, 95% CI = 0.68 to 1.22 vs Tegavivint group mean = 0.011, 95% CI = 0.0012 to 0.056, P < .001), CD44 (control group, mean relative mRNA expression = 1.00, 95% CI = 0.78 to 1.28 vs Tegavivint group mean = 0.30, 95% CI = 0.21 to 0.38, P < .001), and c-Myc (control group, mean relative mRNA expression = 1.00, 95% CI = 0.71 to 1.34 vs Tegavivint group mean = 0.099, 95% CI = 0.066 to 0.15, P < .001) (23–26) (Figure 4F).

To further investigate the efficacy of Tegavivint on OS metastasis, we developed an innovative PDX-derived lung metastasis model (Figure 5A). TCCC-OS84 OS metastatic lung tumor cells were stepwise transferred from the lung of the patient to implantation, and growth in the mouse directly followed by resection and dissociation into single cells for tail vein injection. One week after injection, Tegavivint or vehicle treatment was initiated (Figure 5A). Tegavivint treatment drastically suppressed the metastatic lung tumor growth compared with vehicle treatment (Figure 5, B–D).
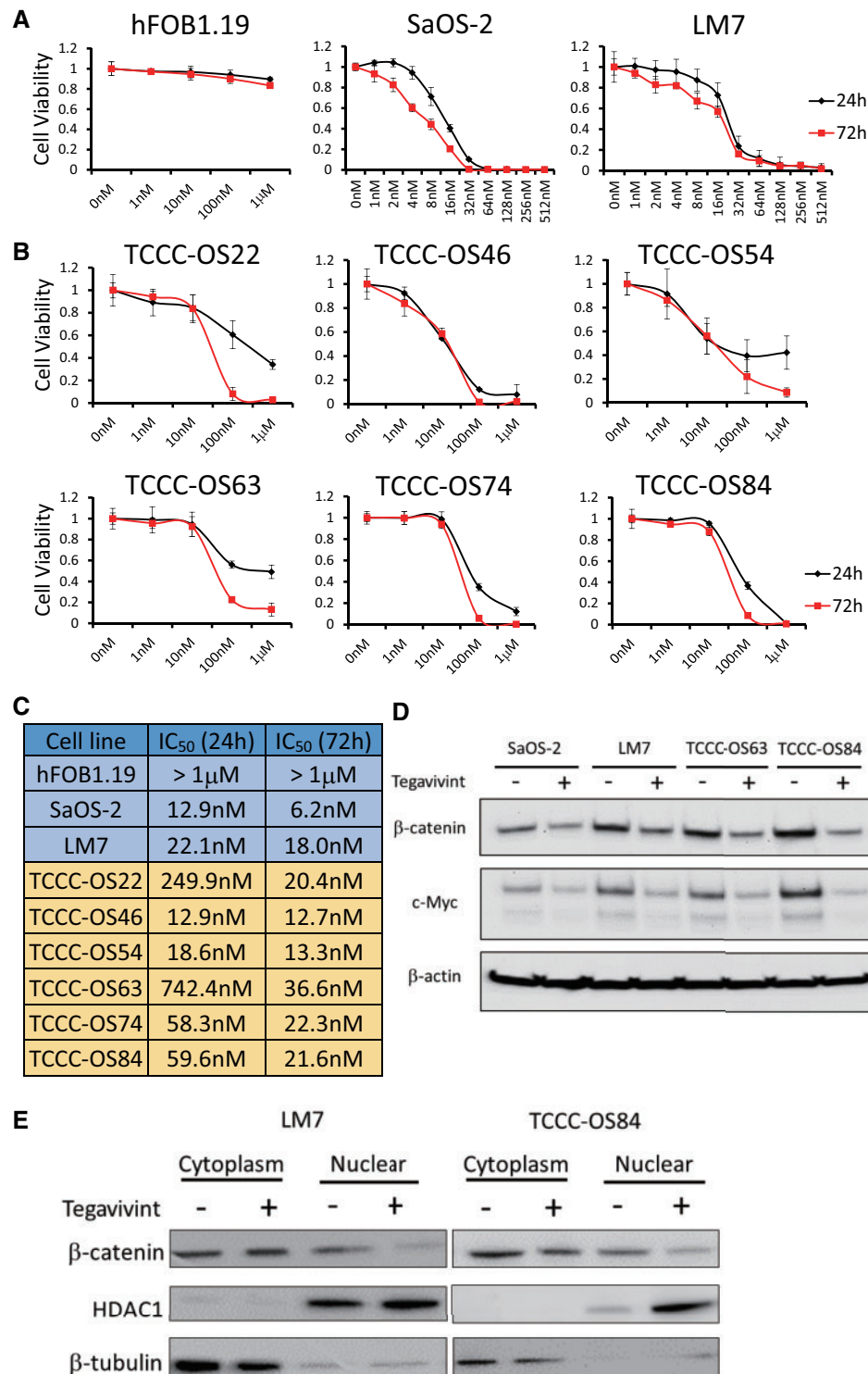
Figure 1. Sensitivity of human fetal osteoblasts and osteosarcoma (OS) cell lines to Tegavivint in vitro. **A)** Nontransformed hFOB1.19 or previously established OS cell lines, or **B)** patient-derived xenograft (PDX)-derived cell lines were treated with increasing concentrations of Tegavivint for up to 72 hours, and cell viability was assessed via CCK-8 assay. **Error bars** represent 95% confidence intervals. **C)** Half-maximal inhibitory concentration (IC_{50}) doses of Tegavivint were calculated based on the results of CCK-8 assay. **D)** Immunoblot analysis of β-catenin and c-Myc in paired primary and lung metastatic OS cell lines was performed by treating each cell line for 24 hours with the appropriate IC_{50} dose of Tegavivint. **E)** Immunoblot analysis of subcellular localization for β-catenin using cell fractions from metastatic LM7 and TCCC-OS84 cells was performed by treating each cell line for 24 hours with the appropriate IC_{50} dose of Tegavivint.
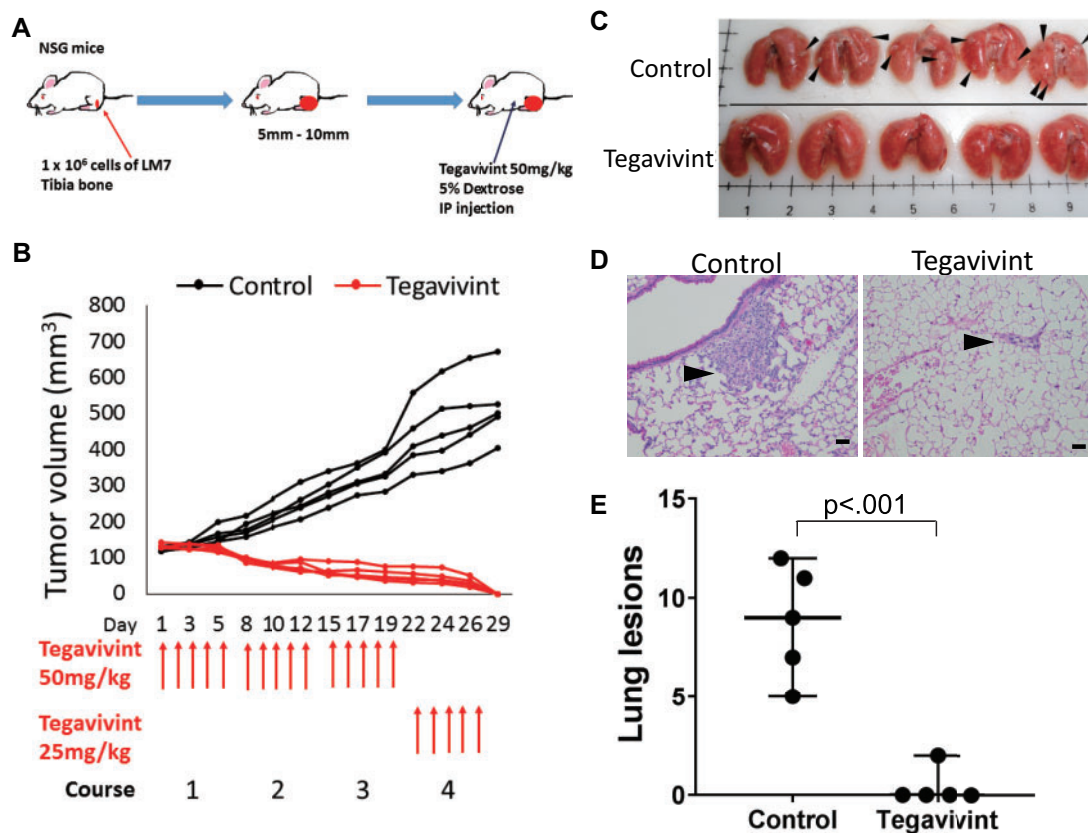
Figure 2. Effect of Tegavivint on orthotopic metastatic osteosarcoma xenograft model. **A)** Schema for the experimental design is shown. LM7 cells were injected into tibia (n = 5/group) in NOD-SCID-IL2$\gamma^{-/-}$ (NSG) mice and treated with vehicle or Tegavivint for 4 weeks. **B)** Orthotopic primary tumor growth curves for each mouse in the control and Tegavivint-treated cohorts are shown. **C)** Images of whole lungs from control and Tegavivint-treated mice are shown. **Black arrowheads** indicate the presence of visible lesions. **D)** Representative hematoxylin and eosin-stained lung sections from control and Tegavivint-treated cohorts are shown. **Black arrowheads** indicate pulmonary lesions. **E)** The number of pulmonary nodules per mouse from control and Tegavivint-treated mice are quantified. Two-sided Student t test was used to determine statistical significance. **Error bars** represent 95% confidence intervals. **Scale bar** = 100 μm.

Effect of Tegavivint on β-Catenin Activity in Lung Metastasis Cells in ex Vivo PuMA Model

To investigate the role of β-catenin activation in OS lung metastasis formation and the mechanism of Tegavivint inhibition of lung metastasis, we transduced LM7 and TCCC-OS84 cells with the 7TGC vector, which consists of 7xTcf-eGFP and SV40-mCherry (Supplementary Figure 2, available online) (27). We recognized lung OS cells by mCherry and β-catenin activation by green fluorescent protein (GFP). After sorting of mCherry-positive cells, we confirmed that activation of Wnt signaling by pretreatment with Wnt3a ligand was suppressed by Tegavivint (Supplementary Figure 2B, available online).

We used the TCCC-OS84-7TGC and LM7-7TGC cell lines in a three-dimensional ex vivo PuMA model (28–34) (Figure 6A and Supplementary Figure 3A, available online). Seven days after sacrifice, lung slices were treated with either vehicle (dimethyl sulfoxide) or 100 nM Tegavivint and maintained in fresh medium for up to 28 days. In the control, tumor cell colonies continued to grow and demonstrate β-catenin activity during metastatic colonization and progression (Figure 6, B and C; Supplementary Figure 3, B and C, available online). The tumor colonies in the Tegavivint-treated samples disappeared by day 14, and recurrence was not detectable. After 28 days, H&E-stained lung sections confirmed tumor cells presence (Figure 6D; Supplementary Figure 3D, available online). The

results support a critical role for Wnt/β-catenin activation in the establishment and progression of pulmonary metastasis and potent antimetastatic activity of Tegavivint via blockade of Wnt/β-catenin activation.

Relationship Between Wnt/β-Catenin Activation, ALDH1, and Metastases in OS

Tumors consist of heterogeneous cell populations, including a subpopulation of cells with stem-cell like features that contribute to tumor and metastasis initiation. Our group and others demonstrated that OS cells with high aldehyde dehydrogenase (ALDH1) activity have enhanced tumor-initiating capacity (35,36). After confirming that Tegavivint can target and eradicate micro- and macrometastatic OS development, we further investigated Wnt activity and molecular signatures in stem cells using metastatic lung models. We examined the differences in the expression of β-catenin, several Wnt target genes, and stem cell markers between the SaOS-2/LM7 and TCCC-OS63/84 paired metastatic cell lines. We observed higher levels of stem cell (ALDH1A1, SOX2, Nanog) and Wnt signaling target genes (CTNNB1, TCF4, c-Myc, CD44) in LM7 and TCCC-OS84 cells (Supplementary Figure 4, available online), implying enhanced Wnt/β-catenin signaling activity in distal metastatic tumor cells compared with primary tumor cells.
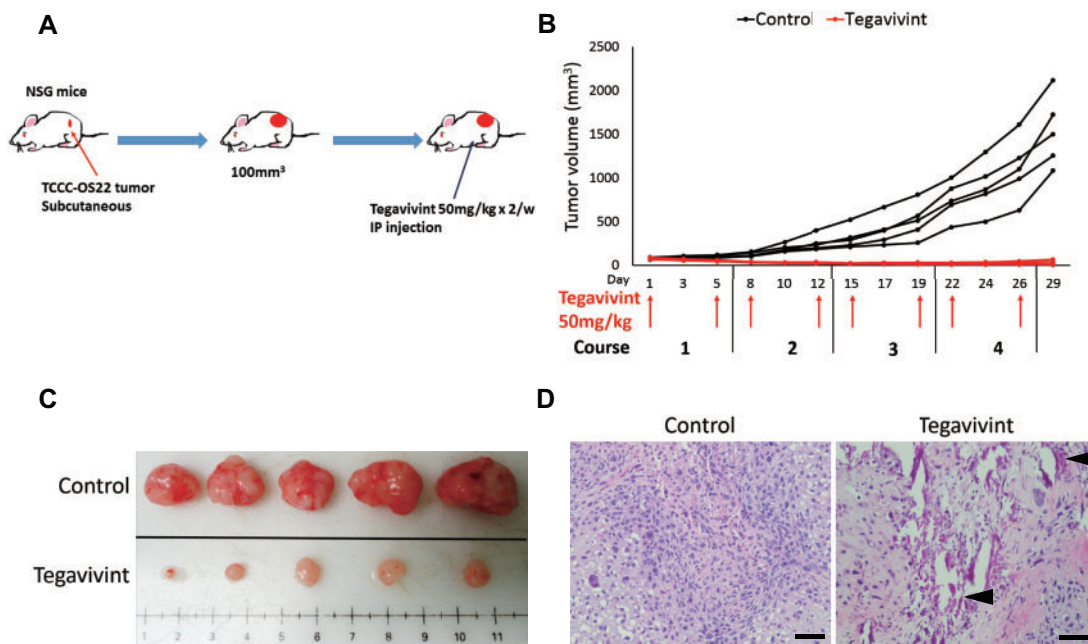
Figure 3. In vivo Tegavivint response of localized osteosarcoma patient-derived xenograft (PDX) model with poor chemotherapeutic response. **A)** Schema of experimental design for the implantation of TCCC-OS22 cells and Tegavivint treatment is shown. When the tumor volume reached 100 mm^3, NOD-SCID-IL2$\gamma^{-/-}$ (NSG) mice (n = 5 per cohort) were treated with either 5% dextrose (vehicle) or Tegavivint twice per week for 4 weeks. **B)** PDX tumor growth curves for control (**black**) and Tegavivint-treated (**red**) mice are shown. **C)** All mice were killed on day 29, and images of each tumor are shown. **D)** Representative hematoxylin and eosin-stained primary tumors from control and Tegavivint-treated mice are shown. **Black arrowheads** indicate area of calcification. **Scale bar** = 100 μm.

Subsequently, we studied the relationship between Wnt/β-catenin signal and stem cell signatures by sorting LM7-7TGC cells following pretreatment with Wnt3a ligand into TCF^{high} and TCF^{low} populations (Supplementary Figure 5A, available online). The expression of downstream Wnt signaling target genes and *ALDH1A1* increased in the TCF^{high} cells (Supplementary Figure 5B, available online), demonstrating the relationship between Wnt/β-catenin activation and ALDH1 expression. Cell viability analysis revealed TCF^{high} cells were more sensitive to Tegavivint than TCF^{low} cells (Supplementary Figure 5C, available online), further validating the mechanism of action.

To further investigate the relationship between ALDH1 and β-catenin activity in metastatic OS, we sorted TCCC-OS84 and LM7 cells into ALDH1^{low} and ALDH1^{high} cells. The ALDH1^{high} cells exhibited higher expression of *CTNNB1*, *TCF4*, *CD44*, and *c-Myc* than ALDH1^{low} cells in both the TCCC-OS84 and LM7 cells (Figure 7, A and B; Supplementary Figure 6, A and B, available online). ALDH1^{high} cells were more sensitive to Tegavivint than ALDH1^{low} cells in vitro (Figure 7C; Supplementary Figure 6C, available online). Furthermore, ALDH1^{high} cells formed more sarcospheres, a surrogate for self-renewal, than ALDH1^{low} cells, and Tegavivint was extremely effective in eliminating the presence of the sarcospheres (Figure 7, D and E). These in vitro results provide convincing evidence there is a relationship between Wnt/β-catenin and ALDH1, which contributes to the stem-cell like phenotypes and metastasis in OS.

Effect of Blockade of the β-Catenin/ALDH1 Axis on Lung Metastases in Vivo

To examine the β-catenin/ALDH1 axis in vivo, we injected via tail vein 1×10^4 ALDH1^{low} and ALDH1^{high} TCCC-OS84 or LM7 cells (Figure 8A; Supplementary Figure 7A, available online).

One week after injection, animals were assigned to receive either vehicle or Tegavivint by i.p. injection twice per week for 4 weeks. The mice were killed after an additional 4 weeks without treatment and evaluated for metastasis. The lungs were removed, fixed with formalin, and stained with H&E for quantitation of metastatic lesions (Figure 8B; Supplementary Figure 7B, available online). The ALDH1^{high} subpopulation formed statistically significantly more lung metastases than the ALDH1^{low} subpopulation (control group, mean lung lesions = 0.5, 95% CI = 0 to 1, vs Tegavivint group mean = 7.3, 95% CI = 4 to 11, P = .001), and Tegavivint was able to eradicate the metastatic potential of both subpopulations (Figure 8C; Supplementary Figure 7C, available online). These findings demonstrate that targeting the β-catenin/ALDH1 axis by Tegavivint diminishes lung metastasis and is a potential viable therapeutic option for controlling metastatic OS.

Modeling the Side Effects of Tegavivint on Bone Length and Density

A large majority of OS cases occur in children and adolescents with an actively developing skeletal system. Because Wnt/β-catenin signaling is active during normal bone development, potential bone-related side effects of Wnt/β-catenin inhibition are of particular concern in the pediatric population. A preliminary side effect profile, including a bone toxicity study, was carried out in adolescent (4-week-old) NSG mice (four per sex, eight per group) treated with either vehicle or Tegavivint via twice weekly i.p. injection for 4 weeks. No differences were found in liver function, blood counts, or other serum clinical pathology parameters between the treatment group and the control group (Supplementary Figure 8, A–C, available online), but a decreased
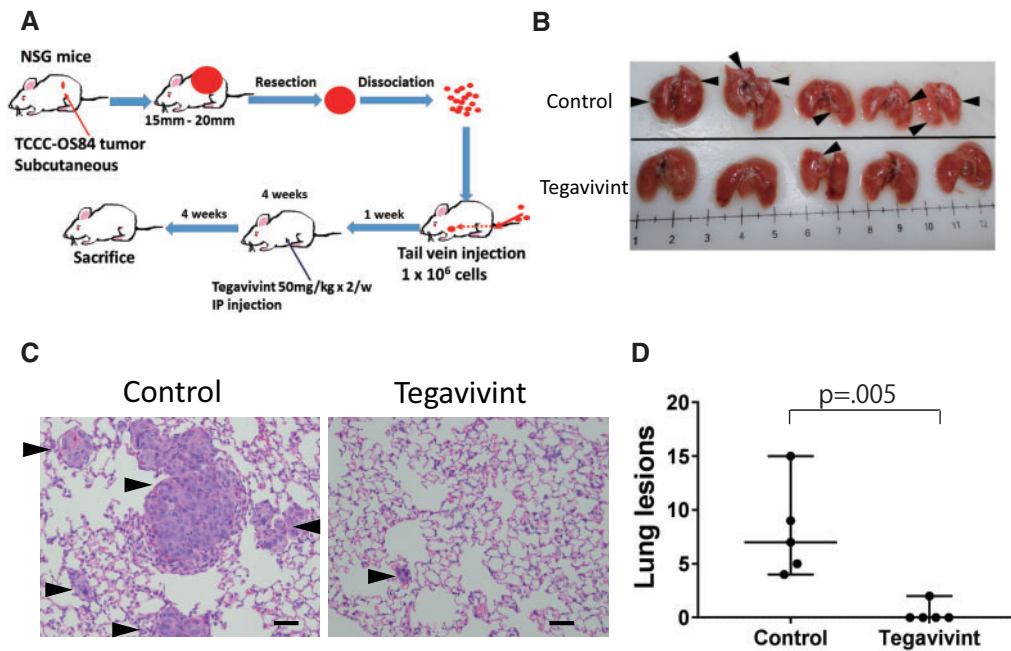
Figure 4. In vivo effect of Tegavivint and combination therapy on osteosarcoma patient-derived xenografts (PDX) development and molecular signatures from cells with inherent high resistance to chemotherapy. A) TCCC-OS63 cells were seeded at the density of 2×10^3 cells per well (n = 8) in 96-well plates and pretreated with 50 nM of doxorubicin (DXR) for 16 hours twice before treatment with different doses of Tegavivint. Data are shown as mean (SD). Two-sided Student t test was used to determine statistical significance. B) Schema for experimental design for PDX TCCC-OS63 single agent and combination therapy is shown. When the tumor volume reached 100 mm^3, NOD-SCID-IL2$\gamma^{-/-}$ (NSG) mice were treated via injection with 5% dextrose (control), DXR only, Tegavivint only, or the combination of DXR and Tegavivint (n = 4/group). C) PDX tumor growth curves for each mouse are shown. D) Kaplan-Meier curves for each cohort were compared using a two-sided log-rank test. P values were adjusted using the Benjamini-Hochberg method, and the pairwise comparisons were considered statistically significant if the adjusted P value was less than .15 (based on q = 0.15). E) Representative hematoxylin and eosin-stained primary tumor section from each group is shown. Calcifications are noted by **black arrowheads**. **Scale bar** = 200 μm. F) Quantitative polymerase chain reaction (qPCR) analysis shows relative mRNA expression levels of *ALDH1A1*, *β-catenin*, *CD44*, and *c-Myc* in each cohort (n = 8). The relative mRNA expression of each gene in control cohort was individually compared with experimental cohorts. Data are shown as median with 95% CI. Two-sided Student t test was used to determine statistical significance.

gain in body weight occurred in the Tegavivint-treated male animals compared with the controls (P < .05) (Supplementary Figure 8D, available online).

Bone histomorphology was evaluated by microCT scanning, and the bone volume-to-total volume ratio and femur bone lengths were calculated using these data. No differences in

Figure 5. In vivo effect of Tegavivint on orthotopic lung patient-derived xenograft (PDX) model. **A)** Schema of single cell dissociation and immediate tail vein injection of primary lung PDX TCCC-OS84 tumor into NOD-SCID-IL2$\gamma^{-/-}$ (NSG) mice (n = 5/group) is shown. **B)** Whole lung images of control and Tegavivint-treated mice are shown. **Black arrowheads** indicate metastatic nodules. **C)** Representative hematoxylin and eosin images for each group is shown. Tumors were observed in each group (**arrowheads**). **Scale bar** = 100 μm. **D)** Average number of pulmonary nodules per three randomly selected sections per mouse was quantified for each experimental group (n = 5). Data are shown as median with 95% confidence interval. Two-sided Student t test was used to determine statistical significance.

bone length were observed, but bone density reduction in the spine and femur (P = .03) was identified in only male mice in the Tegavivint group compared with the control group (Supplementary Figure 8, E and F, available online).

Discussion

Our preclinical data demonstrate the efficacy of Tegavivint in vitro, ex vivo, and in vivo in several models of refractory and metastatic OS. Target inhibition was demonstrated both in vitro and in vivo by the downregulation of Wnt/β-catenin target genes in OS cell cultures and tumor tissues. Furthermore, blockade of Wnt/β-catenin activation by Tegavivint targeted stem-like metastasis-initiating cells and the initiation and progression of lung metastasis. Our results show Tegavivint was effective in vivo in combination with chemotherapy for the treatment of a highly chemoresistant OS tumor model. These results suggest that Tegavivint may have clinical impact for resistant and metastatic OS patients and warrants further clinical investigation.

OS is the most common malignant bone tumor, with stagnant overall survival rates, especially for high-risk patients. Therefore, identifying relevant and effective targets is essential to improve patient outcomes. The Wnt/β-catenin pathway is enhanced in various cancers and has been implicated in tumor progression (2,5–8,11), recurrence (9), metastases (3,10,12,13), and resistance to chemotherapy (4). Our group and others have identified activation of β-catenin transcriptional activity in OS (2–13,37,38).

Chemotherapy can induce stem cell features in tumor cells via activation of the Wnt/β-catenin pathway (31). We

demonstrated enhanced Wnt/β-catenin signaling and ALDH1 activity, suggesting a critical axis involved in the metastasis-initiating and subsequent progression of disseminated OS disease. ALDH1, which is also a marker for tumor-initiating cells for several malignancies, including OS, has been closely associated with tumor progression and metastases (19). ALDH1 was recently reported to be regulated by Wnt/β-catenin signaling in breast cancer (39,40), ovarian cancer (41), and prostate cancer (42). We noted enhanced ALDH1 expression in TCF^{high} cells and enriched expression of β-catenin and associated downstream target genes in ALDH1^{high} cells, which also exhibited enhanced susceptibility to Tegavivint. Future characterization of β-catenin target genes in ALDH^{high} metastatic tumor-initiating cells will provide additional insights into metastatic disease and tumor dormancy.

Because Wnt/β-catenin signaling contributes towards normal osteoblast maturation (18,43), we tested the effects of Tegavivint in a physiologically relevant model of adolescence to examine potential bone-related toxicities. Analysis revealed that Tegavivint induced bone histomorphological changes only in the male cohort. Although the analysis revealed histomorphological differences, these cohorts contained four or fewer samples per group. We intend to expand our cohorts and perform additional bone toxicity studies to confirm these findings. In addition, further detailed studies are essential to delineate the etiology of these findings, but obvious biological differences, including differential hormonal regulation, may contribute to these skeletal aberrations.

Although there are reports of the relationship between genetic mutations in OS progression and specific cell signaling pathways including PI3K/mTOR (44) and insulin-like growth factor pathway (45), there have been rare mutations in Wnt
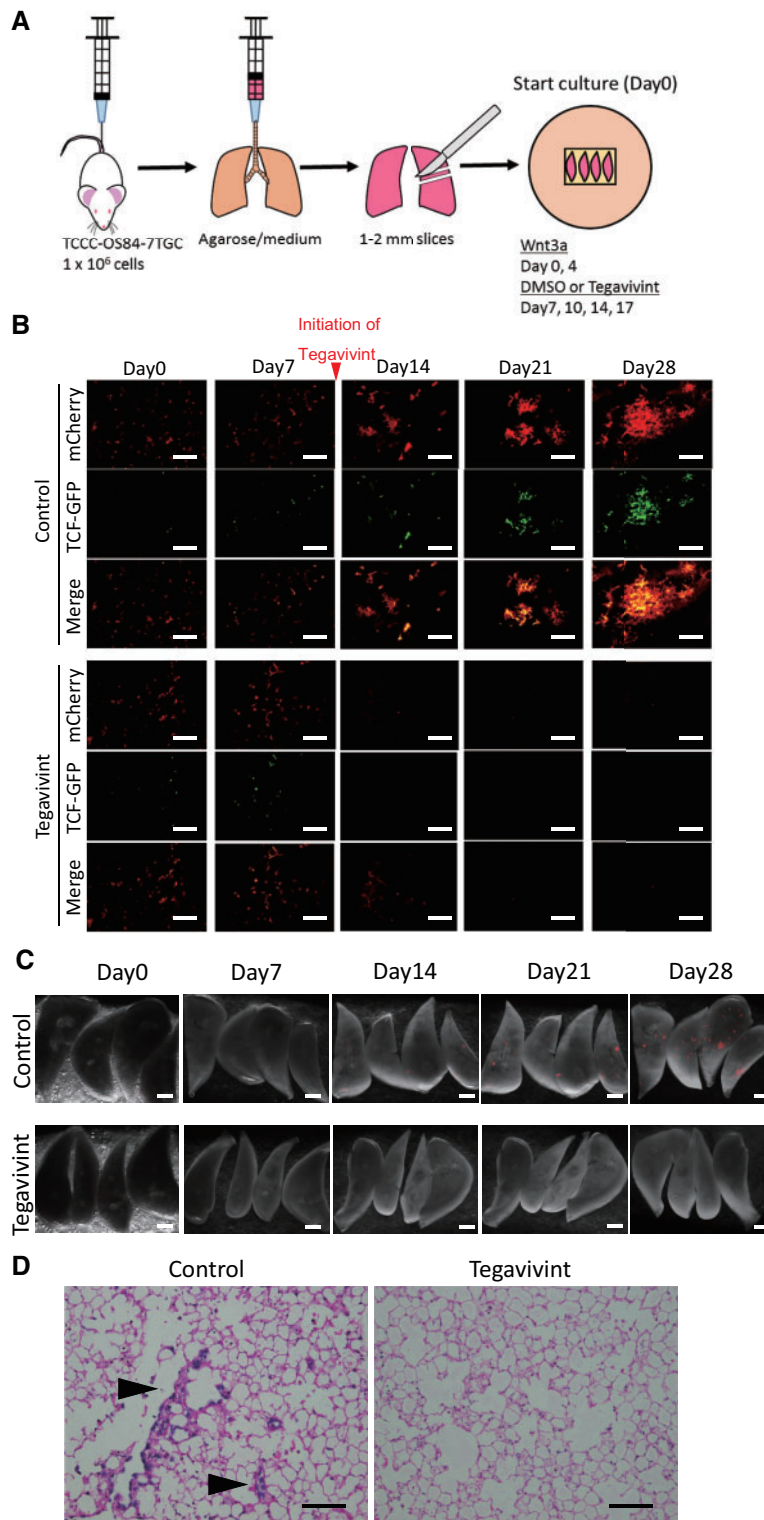
Figure 6. Ex vivo effect of Tegavivint on β-catenin-mediated transcriptional activity in lung-derived TCCC-OS84 cells. **A)** Diagram of pulmonary metastasis assay using the 7TGC-labeled TCCC-OS84-derived cell line is shown. Human recombinant Wnt3a ligand (100 ng/mL) was added to the medium on day 0 and day 4, and dimethyl sulfoxide (DMSO) as a control or Tegavivint (100 nM) was added to the medium on days 7, 10, 14, and 17. **B)** Representative images of lung slices treated with DMSO or Tegavivint. mCherry is constitutively expressed in all tumor cells, and β-catenin/TCF activity is represented with GFP. **Bottom row** for DMSO and Tegavivint treatment represents merged images. **Scale bar** = 100 μm. **C)** Fluorescent images of whole lung lobes in each group is shown. Tumor cells are labeled with mCherry. **Scale bar** = 1 mm. **D)** Representative hematoxylin and eosin-stained lung sections from each group from day 28 are shown, and osteosarcoma cells are noted (**arrowheads**). **Scale bar** = 200 μm.
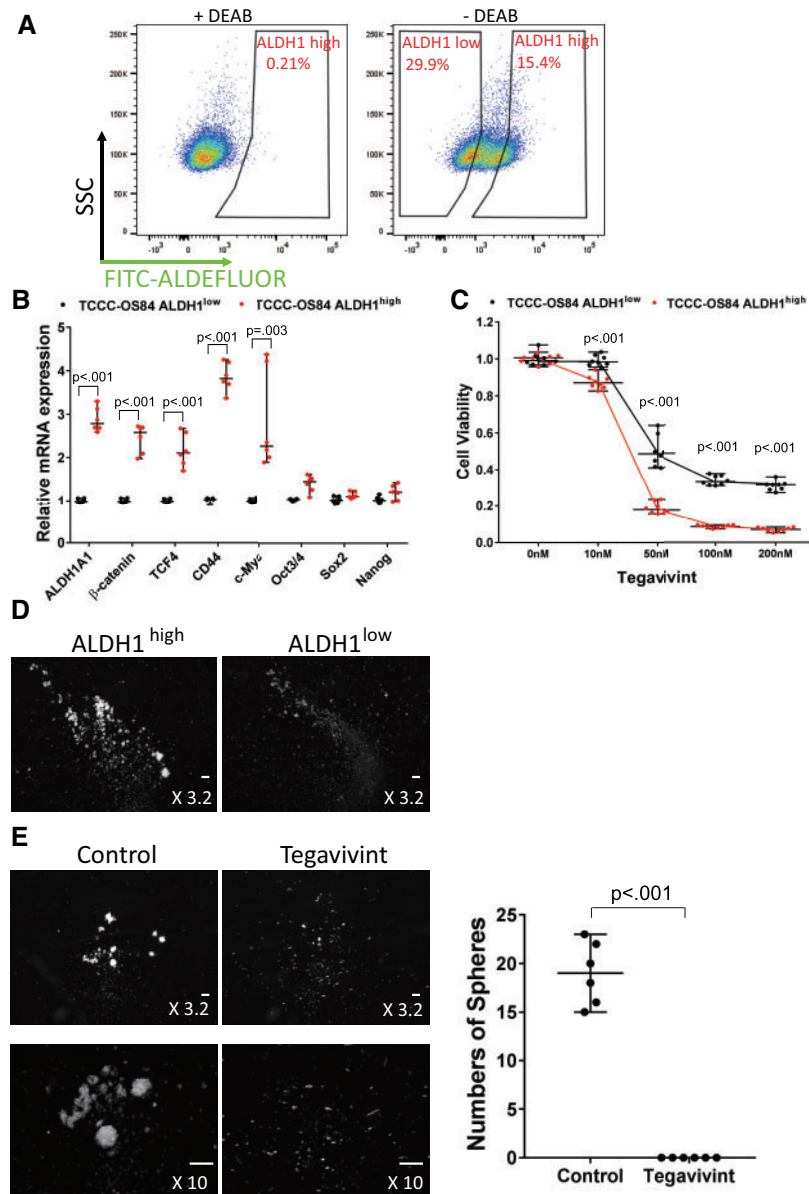
Figure 7. Sensitivity of Tegavivint in metastatic lung patient-derived xenograft-derived ALDH1^{high} cells with respect to viability and self-renewal properties in vitro. **A)** TCCC-OS84 cells were sorted into ALDH1^{high} and ALDH1^{low} populations. N, N-diethylaminobenzaldehyde (DEAB) is an ALDH1 inhibitor used as a negative control. SSC = side scatter. FITC=Fluorescein isothiocyanate **B)** Quantitative polymerase chain reaction (qPCR) analysis for expression of *ALDH1A1*, *β-catenin*, *TCF4*, *CD44*, *c-Myc*, *Oct3/4*, *Sox2*, and *Nanog* in TCCC-OS84 ALDH1^{high} and ALDH1^{low} cell populations (n = 6). Data are shown as median with 95% confidence interval. Two-sided Student *t* test was used to determine statistical significance. **C)** Effect of Tegavivint treatment for 24 hours on cell viability of ALDH1^{high} and ALDH1^{low} cells (n = 8) is shown. Data are shown as median with 95% confidence interval. **D)** Representative images of primary sarcospheres 6 days after seeding ALDH1^{low} or ALDH1^{high} cells are shown. **Scale bar** = 100 μm. **E)** Low- and high-magnification images of secondary sarcospheres 6 days after seeding ALDH1^{high} cells with or without pretreatment with 100 nM Tegavivint are shown. The average number of sarcospheres in each group (n = 6/group) was quantified. Data are shown as median with 95% confidence interval. Two-sided Student *t* test was used to determine statistical significance. **Scale bar** = 100 μm.

signaling components. However, activated mTOR and ERK signaling can crosstalk and activate *β*-catenin (46). Furthermore, a systems biology analysis of genomic and proteomic profiles identified enhanced Wnt signaling in metastatic OS (47). Our accumulated data further corroborate targeting *β*-catenin activity has antitumor and metastatic activity.

Although we have executed a large number of preclinical studies highlighting the efficacy of Tegavivint on high-risk OS conditions through targeting *β*-catenin/ALDH axis, certain limitations remain to our studies. These include elucidating mechanistic insights into the observed side effects as well as additional molecular studies to further augment the pharmacological results we observed. These future studies will enhance our mechanistic and biological insights into high-risk OS.

In conclusion, we demonstrated through extensive in vitro, ex vivo, and in vivo models of high-risk OS that Tegavivint is a promising therapeutic for OS intervention via its inhibition of the *β*-catenin/ALDH1 axis.
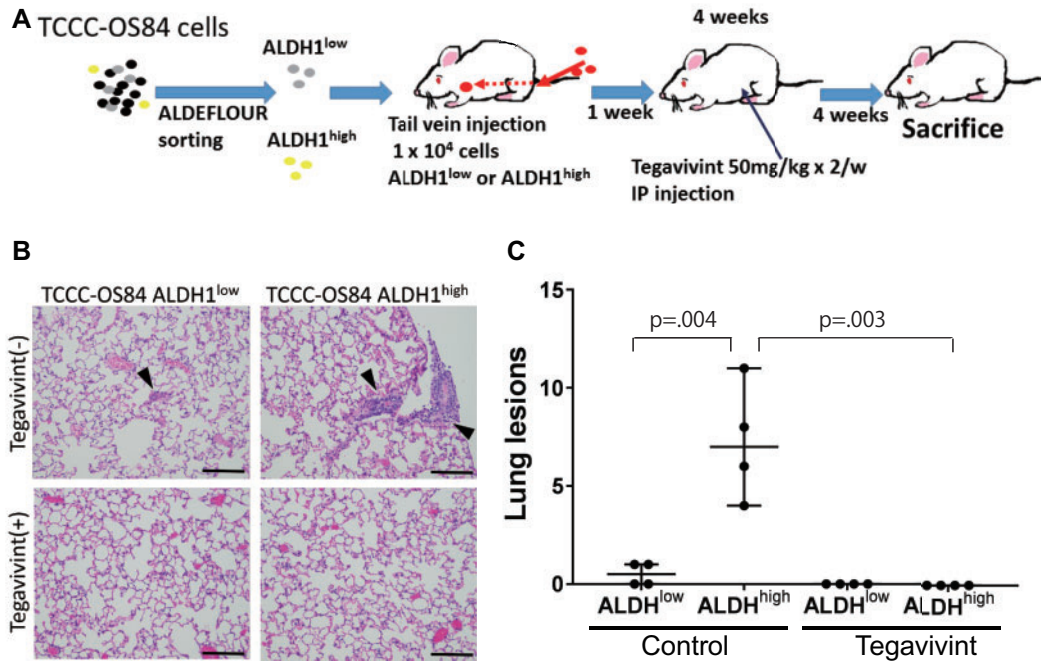
Figure 8. In vivo effect of Tegavivint on metastatic potential of the ALDH1^{high} population of TCCC-OS84 cells. **A)** Schema of experimental approach with tail vein injection of ALDH1^{low} or ALDH1^{high} populations of TCCC-OS84 lung cells and subsequent treatment with Tegavivint is shown. **B)** Representative hematoxylin and eosin-stained lung sections from each cohort are shown. **Scale bar** $= 200\,\mu\text{m}$. **C)** Average number of pulmonary nodules per three randomly selected sections was quantified per mouse (four mice/cohort). Comparison of the ALDH1^{high} without Tegavivint cohort to the other cohorts was performed. Data are shown as median with 95% confidence interval. Wilcoxon rank sum test was used to determine statistical significance.

Funding

Notes

Affiliations of authors: Department of Pediatrics, Texas Children's Cancer and Hematology Center (MN, NR, RS, LK, JTY) and Integrative Molecular and Biological Sciences (YCL, JTY) and Department of Molecular and Human Genetics (BD) and Department of Molecular and Cellular Biology (CC) and Dan L. Duncan Comprehensive Cancer Center (CC, JTY), Baylor College of Medicine, Houston, TX; Iterion Therapeutics, Houston, Texas (RH, JLL).

References

1. Isakoff MS, Bielack SS, Meltzer P, Gorlick R. Osteosarcoma: current treatment and a collaborative pathway to success. *J Clin Oncol*. 2015;33(27):3029–3035.

2. Zhao H, Hou W, Tao J, et al. Upregulation of lncRNA HNF1A-AS1 promotes cell proliferation and metastasis in osteosarcoma through activation of the Wnt/β-catenin signaling pathway. *Am J Transl Res*. 2016;8(8):3503–3512.

3. Han W, Liu J. Epigenetic silencing of the Wnt antagonist APCDD1 by promoter DNA hyper-methylation contributes to osteosarcoma cell invasion and metastasis. *Biochem Biophys Res Commun*. 2017;491(1):91–97.

4. Ma Y, Ren Y, Han EQ, et al. Inhibition of the Wnt-β-catenin and Notch signaling pathways sensitizes osteosarcoma cells to chemotherapy. *Biochem Biophys Res Commun*. 2013;431(2):274–279.

5. Hoang BH, Kubo T, Healey JH, et al. Dickkopf 3 inhibits invasion and motility of saos-2 osteosarcoma cells by modulating the Wnt-β-catenin pathway. *Cancer Res*. 2004;64(8):2734–2739.

6. Zhang W, Duan N, Zhang Q, et al. DNA methylation mediated down-regulation of miR-370 regulates cell growth through activation of the Wnt/β-catenin signaling pathway in human osteosarcoma cells. *Int J Biol Sci*. 2017;13(5):561–573.

7. Hoang BH, Kubo T, Healey JH, et al. Expression of LDL receptor-related protein 5 (LRP5) as a novel marker for disease progression in high-grade osteosarcoma. *Int J Cancer*. 2004;109(1):106–111.

8. Cai Y, Cai T, Chen Y. Wnt pathway in osteosarcoma, from oncogenic to therapeutic. *J Cell Biochem*. 2014;115(4):625–631.

9. Jin H, Luo S, Wang Y, et al. miR-135b stimulates osteosarcoma recurrence and lung metastasis via notch and Wnt/β-catenin signaling. *Mol Ther Nucleic Acids*. 2017;8:111–122.

10. Goldstein SD, Trucco M, Bautista Guzman W, Hayashi M, Loeb DM. A monoclonal antibody against the Wnt signaling inhibitor dickkopf-1 inhibits osteosarcoma metastasis in a preclinical model. *Oncotarget*. 2016;7(16):21114–21123.

11. Brun J, Dieudonne FX, Marty C, et al. FHL2 silencing reduces Wnt signaling and osteosarcoma tumorigenesis in vitro and in vivo. *PLoS One*. 2013;8(1):e55034.

12. Lin CH, Guo Y, Ghaffar S, et al. Dkk-3, a secreted wnt antagonist, suppresses tumorigenic potential and pulmonary metastasis in osteosarcoma. *Sarcoma*. 2013;2013:147541.

13. Wang S, Zhang D, Han S, et al. Fibulin-3 promotes osteosarcoma invasion and metastasis by inducing epithelial to mesenchymal transition and activating the Wnt/β-catenin signaling pathway. *Sci Rep*. 2017;7(1):6215.

14. Tejpar S, Nollet F, Li C, et al. Predominance of beta-catenin mutations and beta-catenin dysregulation in sporadic aggressive fibromatosis (desmoid tumor). *Oncogene*. 1999;18(47):6615–6620.

15. Soldi R, Horrigan SK, Cholody MW, et al. Design, synthesis, and biological evaluation of a series of anthracene-9, 10-dione dioxime b-catenin pathway inhibitors. *J Med Chem*. 2015;58(15):5854–5862.

ARTICLE

16. Fiskus W, Sharma S, Saha S, et al. Pre-clinical efficacy of combined therapy with novel β-catenin antagonist BC2059 and histone deacetylase inhibitor against AML cells. *Leukemia.* 2015;29(6):1267–1278.

17. Savvidou I, Khong T, Cuddihy A, McLean C, Horrigan S, Spencer A. β-Catenin inhibitor BC2059 is efficacious as monotherapy or in combination with proteasome inhibitor bortezomib in multiple myeloma. *Mol Cancer Ther.* 2017; 16(9):1765–1778.

18. Clevers H, Nusse R. Wnt/β-catenin signaling and disease. *Cell.* 2012;149(6): 1192–1205.

19. Yan G, Lv Y, Guo Q. Advances in osteosarcoma stem cell research and opportunities for novel therapeutic targets. *Cancer Lett.* 2016;370(2):268–274.

20. Clarke MF, Fuller M. Stem cells and cancer: two faces of eve. *Cell.* 2006;124(6): 1111–1115.

21. Joeng KS, Lee YC, Lim J, et al. Osteocyte-specific WNT1 regulates osteoblast function during bone homeostasis. *J Clin Invest.* 2017;127(7):2678–2688.

22. Grafe I, Yang T, Alexander S, et al. Excessive transforming growth factor-b signaling is a common mechanism in osteogenesis imperfecta. *Nat Med.* 2014;20(6):670–675.

23. Wielenga VJM, Smits R, Korinek V, et al. Expression of CD44 in apc and tcf mutant mice implies regulation by the WNT pathway. *Am J Pathol.* 1999; 154(2):515–523.

24. Deng Z, Niu G, Cai L, Wei R, Zhao X. The prognostic significance of CD44V6, CDH11, and β-catenin expression in patients with osteosarcoma. *Biomed Res Int.* 2013;2013(2013):1.

25. Ashihara E, Takada T, Maekawa T. Targeting the canonical Wnt/β-catenin pathway in hematological malignancies. *Cancer Sci.* 2015;106(6):665–671.

26. He TC, Sparks AB, Rago C, et al. Identification of c-MYC as a target of the APC pathway. *Science.* 1998;281(5382):1509–1512.

27. Fuerer C, Nusse R. Lentiviral vectors to probe and manipulate the Wnt signaling pathway. *PLoS One.* 2010;5(2):e9370.

28. Ren L, Hong S, Chen QR, et al. Dysregulation of ezrin phosphorylation prevents metastasis and alters cellular metabolism in osteosarcoma. *Cancer Res.* 2012;72(4):1001–1012.

29. Morrow JJ, Mendoza A, Koyen A, et al. mTOR inhibition mitigates enhanced mRNA translation associated with the metastatic phenotype of osteosarcoma cells in vivo. *Clin Cancer Res.* 2016;22(24):6129–6141.

30. Mendoza A, Hong SH, Osborne T, et al. Modeling metastasis biology and therapy in real time in the mouse lung. *J Clin Invest.* 2010;120(8):2979–2988.

31. Hong SH, Ren L, Mendoza A, Eleswarapu A, Khanna C. Apoptosis resistance and PKC signaling: distinguishing features of high and low metastatic cells. *Neoplasia.* 2012;14(3):249–258.

32. Bulut G, Hong SH, Chen K, et al. Small molecule inhibitors of ezrin inhibit the invasive phenotype of osteosarcoma cells. *Oncogene.* 2012;31(3):269–281.

33. Ren L, Hong ES, Mendoza A. Metabolomics uncovers a link between inositol metabolism and osteosarcoma metastasis. *Oncotarget.* 2017;8(24): 38541–38553.

34. Ren L, Mendoza A, Zhu J, et al. Characterization of the metastatic phenotype of a panel of established osteosarcoma cells. *Oncotarget.* 2015;6(30): 29469–29481.

35. Awad O, Yustein JT, Shah P, et al. High ALDH activity identifies chemotherapy-resistant Ewing's sarcoma stem cells that retain sensitivity to EWS-FLI1 inhibition. *PLoS One.* 2010;5(11):e13943.

36. Honoki K, Fujii H, Kubo A, et al. Possible involvement of stem-like populations with elevated ALDH1 in sarcomas for chemotherapeutic drug resistance. *Oncol Rep.* 2010;24(2):501–505.

37. Hu T, Li C, Cao Z, et al. Myristoylated Naked2 antagonizes dishevelled-β-catenin activity by degrading dishevelled-1 at the plasma membrane. *J Biol Chem.* 2010; 285(18):13561–13568.

38. Zhao S, Kurenbekova L, Gao Y, et al. NKD2, a negative regulator of Wnt signaling, suppresses tumor growth and metastasis in osteosarcoma. *Oncogene.* 2015;34(39):5069–5079.

39. Jang GB, Hong I, Kim RJ, et al. Wnt/β-catenin small-molecule inhibitor CWP232228 preferentially inhibits the growth of breast cancer stem-like cells. *Cancer Res.* 2015;75(8):1691–1702.

40. Jang GB, Kim JY, Cho SD, et al. Blockade of Wnt/β-catenin signaling suppresses breast cancer metastasis by inhibiting CSC-like phenotype. *Sci Rep.* 2015;5:12465.

41. Condello S, Morgan CA, Nagdas S, et al. β-Catenin-regulated ALDH1A1 is a target in ovarian cancer spheroids. *Oncogene.* 2015;34(18):2297–2308.

42. Cojoc M, Peitzsch C, Kurth I, et al. Aldehyde dehydrogenase is regulated by β-catenin/TCF and promotes radioresistance in prostate cancer progenitor cells. *Cancer Res.* 2015;75(7):1482–1494.

43. Holmen SL, Zylstra CR, Mukherjee A, et al. Essential role of β-catenin in postnatal bone acquisition. *J Biol Chem.* 2005;280(22):21162–21168.

44. Perry JA, Kiezun A, Tonzi P, et al. Complementary genomic approaches highlight the PI3K/mTOR pathway as a common vulnerability in osteosarcoma. *Proc Natl Acad Sci USA.* 2014;111(51):E5564–E5573.

45. Behjati S, Tarpey PS, Haase K, et al. Recurrent mutation of IGF signaling genes and distinct patterns of genomic rearrangement in osteosarcoma. *Nat Comms.* 2017;8:15936.

46. Liu H, Remedi MS, Pappan KL, et al. Glycogen synthase kinase-3 and mammalian target of rapamycin pathways contribute to DNA synthesis, cell cycle progression, and proliferation in human islets. *Diabetes.* 2009;58(3):663–672.

47. Flores RJ, Li Y, Yu A, et al. A systems biology approach reveals common metastatic pathways in osteosarcoma. *BMC Syst Biol.* 2012;6(1):50.

ARTICLE